



Observation of multiple charge density wave phases in epitaxial monolayer 1T-VSe₂ film

Junyu Zong(宗君宇), Yang Xie(谢阳), Qinghao Meng(孟庆豪), Qichao Tian(田启超), Wang Chen(陈望), Xuedong Xie(谢学栋), Shaoen Jin(靳少恩), Yongheng Zhang(张永衡), Li Wang(王利), Wei Ren(任伟), Jian Shen(沈健), Aixi Chen(陈爱喜), Pengdong Wang(王鹏栋), Fang-Sen Li(李坊森), Zhaoyang Dong(董召阳), Can Wang(王灿), Jian-Xin Li(李建新), and Yi Zhang(张翼)

Citation: Chin. Phys. B, 2022, 31 (10): 107301. DOI: 10.1088/1674-1056/ac5c3e

Journal homepage: <http://cpb.iphy.ac.cn>; <http://iopscience.iop.org/cpb>

What follows is a list of articles you may be interested in

Tip-induced superconductivity commonly existing in the family of transition-metal dipnictides MPn_2

Meng-Di Zhang(张孟迪), Sheng Xu(徐升), Xing-Yuan Hou(侯兴元), Ya-Dong Gu(谷亚东), Fan Zhang(张凡), Tian-Long Xia(夏天龙), Zhi-An Ren(任治安), Gen-Fu Chen(陈根富), Ning Hao(郝宁), and Lei Shan(单磊)

Chin. Phys. B, 2021, 30 (1): 017304. DOI: 10.1088/1674-1056/abccbb

Progress on band structure engineering of twisted bilayer and two-dimensional moiré heterostructures

Wei Yao(姚维), Martin Aeschlimann, and Shuyun Zhou(周树云)

Chin. Phys. B, 2020, 29 (12): 127304. DOI: 10.1088/1674-1056/abc7b6

Epitaxial fabrication of monolayer copper arsenide on Cu(111)

Shuai Zhang(张帅), Yang Song(宋洋), Jin Mei Li(李金梅), Zhenyu Wang(王振宇), Chen Liu(刘晨), Jia-Ou Wang(王嘉鸥), Lei Gao(高蕾), Jian-Chen Lu(卢建臣), Yu Yang Zhang(张余洋), Xiao Lin(林晓), Jinbo Pan(潘金波), Shi Xuan Du(杜世萱), Hong-Jun Gao(高鸿钧)

Chin. Phys. B, 2020, 29 (7): 077301. DOI: 10.1088/1674-1056/ab8db3

Seeing Dirac electrons and heavy fermions in new boron nitride monolayers

Yu-Jiao Kang(康玉娇), Yuan-Ping Chen(陈元平), Jia-Ren Yuan(袁加仁), Xiao-Hong Yan(颜晓红), Yue-E Xie(谢月娥)

Chin. Phys. B, 2020, 29 (5): 057303. DOI: 10.1088/1674-1056/ab7e9e

General principles to high-throughput constructing two-dimensional carbon allotropes

Qing Xie(谢庆), Lei Wang(王磊), Jiangxu Li(李江旭), Ronghan Li(李荣汉), Xing-Qiu Chen(陈星秋)

Chin. Phys. B, 2020, 29 (3): 037306. DOI: 10.1088/1674-1056/ab6c4b

Observation of multiple charge density wave phases in epitaxial monolayer 1T-VSe₂ film

Junyu Zong(宗君宇)¹, Yang Xie(谢阳)¹, Qinghao Meng(孟庆豪)¹, Qichao Tian(田启超)¹, Wang Chen(陈望)¹, Xuedong Xie(谢学栋)¹, Shaoen Jin(靳少恩)¹, Yongheng Zhang(张永衡)¹, Li Wang(王利)², Wei Ren(任伟)², Jian Shen(沈健)², Aixi Chen(陈爱喜)², Pengdong Wang(王鹏栋)², Fang-Sen Li(李坊森)², Zhaoyang Dong(董召阳)³, Can Wang(王灿)^{1,4}, Jian-Xin Li(李建新)^{1,4,†}, and Yi Zhang(张翼)^{1,4,‡}

¹National Laboratory of Solid State Microstructure, School of Physics, Nanjing University, Nanjing 210093, China

²Vacuum Interconnected Nanotech Workstation (Nano-X), Suzhou Institute of Nano-Tech and Nano-Bionics (SINANO), Chinese Academy of Sciences, Suzhou 215123, China

³Department of Applied Physics, Nanjing University of Science and Technology, Nanjing 210094, China

⁴Collaborative Innovation Center of Advanced Microstructures, Nanjing University, Nanjing 210093, China

(Received 15 January 2022; revised manuscript received 26 February 2022; accepted manuscript online 10 March 2022)

As a special order of electronic correlation induced by spatial modulation, the charge density wave (CDW) phenomena in condensed matters attract enormous research interests. Here, using scanning-tunneling microscopy in various temperatures, we discover a hidden incommensurate stripe-like CDW order besides the $(\sqrt{7} \times \sqrt{3})$ CDW phase at low-temperature of 4 K in the epitaxial monolayer 1T-VSe₂ film. Combining the variable-temperature angle-resolved photoemission spectroscopic (ARPES) measurements, we discover a two-step transition of an anisotropic CDW gap structure that consists of two parts Δ_1 and Δ_2 . The gap part Δ_1 that closes around ~ 150 K is accompanied with the vanish of the $(\sqrt{7} \times \sqrt{3})$ CDW phase. While another momentum-dependent gap part Δ_2 can survive up to ~ 340 K, and is suggested to the result of the incommensurate CDW phase. This two-step transition with anisotropic gap opening and the resulted evolution in ARPES spectra are corroborated by our theoretical calculation based on a phenomenological form for the self-energy containing a two-gap structure $\Delta_1 + \Delta_2$, which suggests different forming mechanisms between the $(\sqrt{7} \times \sqrt{3})$ and the incommensurate CDW phases. Our findings provide significant information and deep understandings on the CDW phases in monolayer 1T-VSe₂ film as a two-dimensional (2D) material.

Keywords: charge density waves, VSe₂, band structures, STM, ARPES

PACS: 73.20.Mf, 73.20.At, 73.61.-r

DOI: 10.1088/1674-1056/ac5c3e

1. Introduction

In recent years, the discovery of plentiful two-dimensional (2D) materials brings new platform for studying novel phenomena in condensed matters.^[1–5] Among the 2D materials family, transition metal chalcogenides (TMDCs) attract enormous research interests due to the abundant variety and properties.^[1,6–12] For examples, the monolayer NbSe₂ and FeSe were found to host superconductivity;^[11–13] the monolayer 1T'-WSe₂ and 1T'-WTe₂ were found to be 2D topological insulators and exhibit quantum spin Hall effect;^[7,14–16] the monolayer TiSe₂, TaSe₂ show CDWs with different orders,^[17,18] which became a typical research platform to understand the correlations between electrons and phonons.^[10,19–23] Notably, VSe₂ was found to host various CDW phases. In bulk 1T-VSe₂, $(4 \times 4 \times 3)$ CDW order has been observed below the transition temperature $T_C = 110$ K and its mechanism is suggested as the three-dimensional (3D) Fermi surface nesting.^[24–26] For the monolayer 1T-VSe₂, the coexisting of $(\sqrt{7} \times \sqrt{3})$ and $(2 \times \sqrt{3})$ CDW phases were observed at low temperatures (~ 76 K).^[27,28]

Besides, more complicated CDW phases and corresponding wave vectors were suggested in monolayer 1T-VSe₂ at various temperatures.^[29] Moreover, with angle-resolved photoemission spectroscopic (ARPES) measurements, an asymmetric CDW gap structure accompanied with the CDW phase transition in monolayer 1T-VSe₂ was also reported.^[27,30–32] Till now, although the coexisting of multiple CDW orders is ubiquitous in monolayer 1T-VSe₂, the physical mechanism and a clear description on the CDW phase transitions are still not received unified explanations yet.

Combining the *in-situ* variable-temperature (VT) ARPES and scanning-tunneling microscopic (STM) techniques, here we investigate the multiple CDW phases and their transitions with temperatures in the monolayer 1T-VSe₂ film grown on bilayer graphene (BLG) substrate by molecular beam epitaxial (MBE) method. We found that besides the already reported $(\sqrt{7} \times \sqrt{3})$ CDW reconstruction, another hidden incommensurate CDW phase with period of $\sim 2a$ can coexist with it at ~ 4 K in monolayer 1T-VSe₂ film. As a consequence of the interference between these two CDW phases,

[†]Corresponding author. E-mail: jxli@nju.edu.cn

[‡]Corresponding author. E-mail: zhangyi@nju.edu.cn

the coexistence of $(\sqrt{7} \times \sqrt{3})$ and $(2 \times \sqrt{3})$ reconstruction as observed before can also be found but in short range. Using VT-STM and room-temperature (RT) STM, we found that the $(\sqrt{7} \times \sqrt{3})$ phase will vanish at ~ 165 K but the incommensurate CDW phases become more complicated and can survive up to room-temperature of 300 K. Through the analysis of the CDW gap evolutions at different momentum positions from the VT-ARPES spectra, we found that the CDW gap along the Γ - M direction exhibits a monotonic temperature dependence and vanishes at ~ 150 K, associated with the disappearance of the $(\sqrt{7} \times \sqrt{3})$ reconstruction observed by STM. Along the M - K direction, the CDW gap is also reduced with temperature, but does not vanish at 150 K, instead it extends to ~ 343 K. Combining with the theoretical calculations using a phenomenological form for the self-energy containing a two-gap structure, we show that the CDW gap exhibits highly anisotropic momentum and temperature dependence, and shows a two-step transition along the M - K direction. We suggest the distinct two parts in the two-gap structure are related with the $(\sqrt{7} \times \sqrt{3})$ CDW phase and incommensurate stripe-like CDW phases, and they may process different physical mechanism behind.

2. Methods

The MBE growth and experimental measurements of the 1T-VSe₂ films were performed in a combined MBE-STM-ARPES ultra-high vacuum (UHV) system with a base pressure of $\sim 2 \times 10^{-10}$ mbar (1 bar = 10⁵ Pa). The STM in the MBE-STM-ARPES system is a Pan-style one and performed at room-temperature. The BLG substrate was obtained by flash-annealing the 4H-SiC (0001) wafer to ~ 1250 °C for 60 cycles.^[33] The V flux was produced from an electron-beam evaporator. The high purity Se (99.9995%) was evaporated from a standard Knudsen cell. The BLG substrate was kept at 280 °C during the growth. The surface morphology was characterized by the *in-situ* reflection high-energy electron diffraction RHEED and RT-STM.

The *in-situ* x-ray photoelectron spectroscopy (XPS) and VT-ARPES measurements were performed via a shared Scienta Omicron DA30L analyzer. The monochromatic x-ray (SIGMA) was generated from an Al electrode excitation source (Al_α, 1486.7 eV), and the ultraviolet (UV) light source was generated by a helium lamp (Fermi instruments) with a SPECS monochromator (He I, 21.218 eV). The samples were cooled down to ~ 7 K by a close-cycle cryogenerator during the measurements, and the sample temperature can be controlled by an *in-situ* inner heater in the manipulator.

The ultra-low-temperature (ULT) STM, VT-STM, and variable-temperature low-energy electron diffraction (VT-LEED) were performed *ex-situ* at Nano-X, Suzhou Institute of Nano-Tech and Nano-Bionics (SINANO), China. The ULT-STM is the UNISOKU Co, USM 1300 with lowest temperature of ~ 4 K. The VT-STM is the Scienta Omicron Co,

VT-AFM XA50/500 with variable temperature operation from 30 K to 300 K. The VT-LEED is the Scienta Omicron Co, LEED 600 MCP with variable temperature operation from 80 K to 300 K.

The first-principles calculations were performed using the QUANTUM ESPRESSO package base on density functional theory (DFT).^[34] The generalized gradient approximation with the Perdew–Burke–Ernzerhof functional was used to describe the electron exchange and correlation effects.^[35] A plane-wave energy cutoff of 80 Ry (1 Ry = 13.6055923 eV) and a $16 \times 16 \times 1$ k mesh was employed. Freestanding films were modeled with a 23-Å vacuum gap between adjacent layers in the supercell. The in-plane lattice parameter a was fixed to the experimentally reported value of 3.35 Å.^[36] Structures were fully optimized until ionic forces and energy difference are less than 10^{-3} eV/Å and 10^{-5} eV.

3. Results and discussion

3.1. The hidden incommensurate CDW phase in monolayer VSe₂

The structure of the 1T-VSe₂ unit cell is represented as a ball and stick model shown in Fig. 1(a). The triangle formed by the top layer of Se atoms is rotated by 180° relative to the bottom Se layer. The RHEED image of a monolayer 1T-VSe₂ film grown on BLG substrate is shown in the upper panel of Fig. 1(b). The sharp RHEED patterns prove that the film was well-crystallized. In the lower panel of Fig. 1(b), the XPS spectrum shows the characterized binding energies of Se 3d_{5/2} (~ 56 eV), Se 3d_{3/2} (~ 57 eV), V 2p_{3/2} (~ 512 eV), and V 2p_{1/2} (~ 520 eV) orbitals, indicating our film is indeed consisted of V and Se atoms.

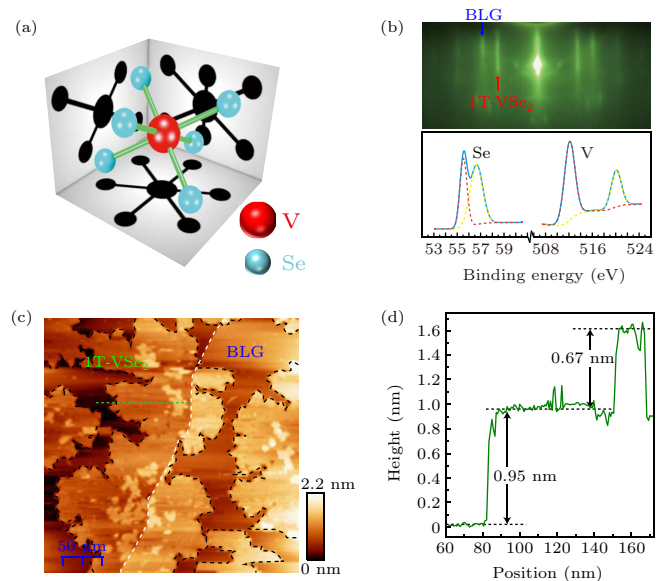


Fig. 1. (a) The structure of the 1T-VSe₂ unit cell. (b) RHEED pattern (upper panel) and XPS spectrum (lower panel) of the monolayer 1T-VSe₂ grown on BLG substrate. (c) STM image (300 nm \times 300 nm) scanned at room-temperature. Scanning parameters: $V_{\text{bias}} = 1$ V, $I_t = 100$ pA. The white dashed line indicates the terrace step of the BLG/SiC(0001) substrate, and the black dashed lines depict the edges of the grown VSe₂ domains. (d) The height profile line along the green dashed line in panel (c).

To further determine the surface morphology of the grown film, we took a $300 \text{ nm} \times 300 \text{ nm}$ STM image scanned at room-temperature [Fig. 1(c)]. The grown 1T-VSe₂ film formed large-scale flat monolayer domains with a coverage of $\sim 80\%$. Few bilayer 1T-VSe₂ islands were formed on the monolayer 1T-VSe₂ surface, but they will not affect our VT-ARPES and VT-STM measurements due to their rather small sizes. From the height profile line shown in Fig. 1(d), we can see that the height of second 1T-VSe₂ layer island to the monolayer domain is about $\sim 0.67 \text{ nm}$, which agree with the lattice constant c of the 1T-VSe₂ monolayer.^[36] However, the height of the monolayer 1T-VSe₂ to the BLG substrate is obviously larger as $\sim 0.95 \text{ nm}$, which is due to the large interlayer spacing between the TMDCs film and BLG substrate.^[29,37,38]

Figure 2(a) is the atom-resolved STM image on the monolayer 1T-VSe₂ taken at $\sim 4 \text{ K}$. The typical CDW reconstructions that are same to previous reports can be clearly observed.^[27–29,31] We found that these CDW reconstructions are consisted of the period of $(\sqrt{7} \times \sqrt{3})$ depicted by the red dashed lines and the period of $(2 \times \sqrt{3})$ depicted by the blue dashed lines, but both these two CDW periods are in short range. To better understand these CDW periods in monolayer 1T-VSe₂, we took fast Fourier transform (FFT) shown in Figs. 2(d) and 2(g), which contains complicated diffraction spots depicted by the black/blue/red circles in Fig. 2(g). In previous reports, different interpretations on these spots were suggested.^[27,29,31] Here we found that the six spots in the black circles show wave vector of $q_0 = (2/\sqrt{3}) \cdot (1/a)$ (where $a = 3.35 \text{ \AA}$ is the in-plane lattice constant of monolayer 1T-VSe₂), which is originated from the intrinsic (1×1) lattice of monolayer 1T-VSe₂. While the spots in the red circles constitute a period grid [red dashed grid in Fig. 2(g)] with wave vectors of $q_1 \approx (1/\sqrt{7})q_0$ and $q_2 \approx (1/\sqrt{3})q_0$, representing the short-range $(\sqrt{7} \times \sqrt{3})$ CDW reconstruction. However, unlike usual CDWs, the rest spots interlacing with the red grid constitute two period grids [blue dashed grids in Fig. 2(g)]. Interestingly, these two blue grids are also consisted of wave vectors of q_1 and q_2 , but with shifts of $\pm q_3$ to the zero point. The $q_3 \approx (1/2)q_0$ may represent the period of $\sim 2a$ [blue dashed lines in Fig. 2(a)] in the $(2 \times \sqrt{3})$ reconstruction. By now, all the diffraction spots in the FFT image can be well interpreted by these three $(\sqrt{7} \times \sqrt{3})$ grids with shifts of $\pm q_3/0$ to the zero point. Notably, the wave vector q_3 shows a small mis-angle of $\sim 11^\circ$ to the (1×1) wave vector (green dashed line), suggesting the existing of a hidden incommensurate CDW phase with period of $\sim 2a$. Thus, the interference between the $(\sqrt{7} \times \sqrt{3})$ and the incommensurate $\sim 2a$ CDW phases in fact results in the short-range $(\sqrt{7} \times \sqrt{3})$ and $(2 \times \sqrt{3})$ CDW reconstructions in real space in Fig. 2(a).

Figure 2(b) is the atom-resolved STM image on monolayer 1T-VSe₂ taken at 165 K . Obviously, the $(\sqrt{7} \times \sqrt{3})$ CDW

reconstruction disappears, only a stripe-like incommensurate CDW phase (depicted by the blue dashed lines) is left. These stripes show an average spacing of $\sim 2a$ and a mis-angle of $\sim 15^\circ$ to the (1×1) lattice, and are also in short range. In the FFT image shown in Figs. 2(e) and 2(h), the $(\sqrt{7} \times \sqrt{3})$ wave vectors of q_1 and q_2 disappear. However, the wave vector $q_3 \approx (1/2)q_0$ still exists with a slightly different mis-angle of $\sim 15^\circ$ [same to the mis-angle in real space image of Fig. 2(b)], and more incommensurate wave vectors (*e.g.* $q_4 \approx (1/4.2)q_0$) emerge. Unfortunately, we are unable to attribute these spots to a period grid strictly, but they are located along the blue dashed lines with spacing of $q_3 \approx (1/2)q_0$. Therefore, we suggest these spots and incommensurate wave vectors represent the stripe-like incommensurate ($\sim 2a$) CDW phase in short range. Notably, similar stripe-like incommensurate CDW phases were widely observed in the 1T-TaS₂,^[39] 1T-TaSe₂,^[40,41] LaTe₂,^[42] TbTe₃,^[43] SmTe₃,^[44] Ta₄Pd₃Te₁₆,^[45] NdO_{1-x}F_xBiS₂,^[46] and cuprates.^[47]

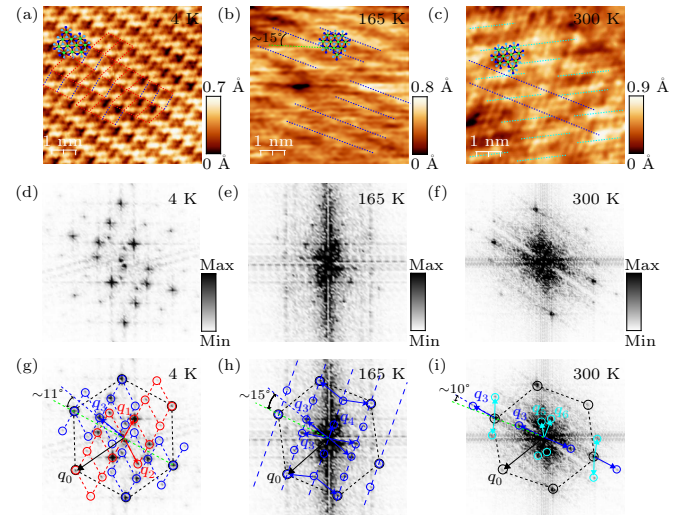


Fig. 2. (a)–(c) The atom-resolved STM images ($6 \text{ nm} \times 6 \text{ nm}$) obtained at (a) 4 K , (b) 165 K , and (c) 300 K , respectively. Scanning parameters: (a) $V_{\text{bias}} = 1 \text{ V}$, $I_t = 200 \text{ pA}$; (b) $V_{\text{bias}} = 0.1 \text{ V}$, $I_t = 3 \text{ nA}$; (c) $V_{\text{bias}} = 0.3 \text{ V}$, $I_t = 1 \text{ nA}$. The green, blue, and cyan dots in the lattice model represent the V, top layer Se, and bottom layer Se atoms in 1T-VSe₂, respectively. The red dashed lines in panel (a) indicate the $(\sqrt{7} \times \sqrt{3})$ CDW reconstruction, and the blue dashed lines in panel (a) indicate the period of $\sim 2a$. (d)–(f) The corresponding FFT images of panels (a)–(c), respectively. (g)–(i) The analysis of the FFT patterns shown in panels (d)–(f).

When the temperature rises to room-temperature of 300 K , the RT-STM image in Fig. 2(c) shows that the stripe-like incommensurate CDW phase in short range still exists but exhibits different formations. In the FFT image shown in Figs. 2(f) and 2(i), we can still observe the wave vector $q_3 \approx (1/2)q_0$ with a mis-angle around $\sim 10^\circ$, accompanied with other different incommensurate wave vectors (*e.g.* $q_5 \approx (1/3.2)q_0$, $q_6 \approx (1/2.7)q_0$). These newly emerged wave vectors may represent the short stripes depicted by the cyan dashed lines in Fig. 2(i), while the incommensurate ($\sim 2a$) CDW order with wave vector $q_3 \approx (1/2)q_0$ can be found by the blue dashed lines but is not very obvious.

From the above analysis on the atom-resolved STM images and their FFT images, we suggest the coexisting of the $(\sqrt{7} \times \sqrt{3})$ and a hidden incommensurate ($\sim 2a$) CDW phases in monolayer 1T-VSe₂ at ultra-low temperature of 4 K. The $(\sqrt{7} \times \sqrt{3})$ phase will disappear at 165 K, implying that a CDW transition happens below 165 K. Considering the observation of the $(\sqrt{7} \times \sqrt{3})$ phase at 76 K in previous reports,^[27,28,31] here we suggest the CDW phase transition point is between 76 K to 165 K.

To confirm that the reconstructions shown in the STM images are indeed originated from the CDW phases rather than the lattice structure phase transition, we carried out the low-energy electron diffraction (LEED) taken at various temperatures. Figure 3 shows the LEED images taken at 80 K, 200 K, and 300 K. The (1×1) diffraction patterns from the BLG substrate can be clearly observed and are depicted by the white dashed hexagons. Besides, the spots depicted by the red dashed hexagons are originated from the (1×1) lattice of the grown 1T-VSe₂. Feng *et al.* have reported that a weak diffraction pattern of the CDW order in monolayer 1T-VSe₂ can be observed in the LEED taken at 40 K,^[30] but here we did not find any features on the CDW reconstructions. This may be due to the relative poorer resolution limit of our LEED system. However, for the TMDCs materials, the crystalline structure phase transitions usually can be easily distinguished by the electron diffraction method, *e.g.*, the 2H to 1T' phase transition in monolayer WSe₂ will produce an additional pattern in the electron diffraction images.^[37,48] Here, except the (1×1) pattern from the 1T-VSe₂, no other diffraction pattern was found in the VT-LEED measurements, indicating that no crystalline phase transition happens in 1T-VSe₂. Thus, the stripe-like CDW structures observed in STM are not from crystalline phase transition such as 1T to 1T'.

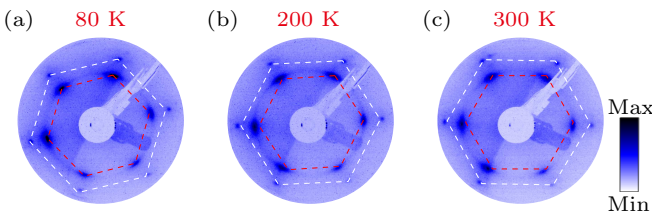


Fig. 3. (a)–(c) LEED images of the grown monolayer 1T-VSe₂ film on BLG substrates taken at (a) 80 K, (b) 200 K, and (c) 300 K, respectively. The white dashed hexagons indicate the (1×1) diffraction patterns from the BLG substrate, and the red dashed hexagons indicate the (1×1) diffraction patterns from the grown 1T-VSe₂ film.

3.2. Two-step CDW gap structure transition

To investigate the CDW transition with temperature in detail, we performed VT-APRES measurements to study how the band structures evolve with the CDW transition in the monolayer 1T-VSe₂ film at various temperatures.

Figure 4(a) shows the constant-energy-mapping at the binding energy of -0.1 eV below the Fermi level at the temperature of 7 K. Six elliptic pockets can be clearly observed

around the six M points of the hexagonal Brillouin zone (BZ), which is consistent with the calculated Fermi surface from the previous reports.^[36,49,50] Figure 4(b) shows the ARPES spectra along the Γ – M – K directions. We can see that the band disperses towards the Fermi level at the momentum positions marked by the red α point and blue β point, at which the CDW gaps can be observed and extracted from the symmetrized energy distribution curves (EDCs) of the ARPES spectra. Figures 4(c) and 4(d) show the symmetrized EDCs with subtraction of Fermi function at the momentum positions of the α and β points, respectively. These EDCs were taken at temperatures from 7 K to 340 K. Usually we can take the distance between the two symmetric peaks to be twice of the CDW gap ($2 \times \Delta$).^[31] When the temperature rises, the peaks of the EDC will gradually flatten around the 0 eV, indicating that the CDW gap closes. The temperature dependences of the CDW gaps extracted from Figs. 4(c) and 4(d) were plotted in Figs. 4(e) and 4(f). Remarkably, we found that the gaps at different momentum positions show quite distinct behaviors. At the momentum position marked as the α point near the Γ point, the CDW gap exhibits a monotonic temperature dependence and gradually decreases from $\sim 30 \pm 5$ meV to zero around ~ 150 K; while at the momentum position marked as the β point, the CDW gap decreases from $\sim 62 \pm 5$ meV to $\sim 30 \pm 8$ meV at ~ 150 K, then it shows a stable decrease with temperature in an extended range and finally begins to drop since ~ 310 K, showing a closing trend around ~ 340 K. In Fig. A1 in Appendix A, we also plot the zoom-in symmetrized EDCs at the α and β points near the transition temperature of ~ 150 K and ~ 340 K to show the close and the closing trend of the CDW gap. The error bars of the gaps data are set as $\sqrt{(\frac{1}{2}k_B T)^2 + (\epsilon_s)^2}$, where k_B is the Boltzmann constant, ϵ_s is the resolution limit (~ 5 meV) of the ARPES system.

According to our above STM results, one may ascribe the low temperature gap as resulting from the $(\sqrt{7} \times \sqrt{3})$ CDW phase, while the intermediate temperature gap as from the stripe-like incommensurate CDW phase. Therefore, we suggest a two-gap formula at the mean-field level to describe the temperature dependence of the CDW gap,^[31]

$$\Delta_i(T) \propto \tanh \left(A \sqrt{\frac{T_{Ci}}{T} - 1} \right) \Theta(T_{Ci} - T),$$

$$i = 1, 2, \quad (1)$$

where A is a proportional constant and Θ is the unit step function. At the momentum position marked as the α point near the Γ point, only Δ_1 is included. The fitting result to the experimental data is shown in Fig. 4(e) as the red line, which shows a well agreement to the original experimental data. According to the fitting result, we get $\Delta_1 = 30 \pm 6$ meV and $T_{C1} = 151 \pm 6$ K. At the momentum position marked as the β point, both Δ_1 and Δ_2 are included, and we use $\Delta(T) = \Delta_1(T) + \Delta_2(T)$ to fit the

data. The fitting result is shown as the red line in Fig. 4(f), we get a very good fitting result with $\Delta_1 = 32 \pm 2$ meV, $\Delta_2 = 30 \pm 1$ meV, $T_{C1} = 153 \pm 2$ K, and $T_{C2} = 343 \pm 2$ K. The errors of the fitting results are set in 68% confidence interval. Here the two fitting results of Δ_1 and T_{C1} are within the fitting errors. The combination of the experimental results and the theoretical fitting indicates that there exist two distinct CDW gaps with highly anisotropic gap distributions in the momentum space, in particular a two-step gap transition at the β

point along the M - K direction in the monolayer 1T-VSe₂, one is suggested to be associated with the $(\sqrt{7} \times \sqrt{3})$ CDW with a transition temperature T_{C1} of ~ 151 K (denoted by Δ_1), while another may be associated with the stripe-like incommensurate CDW phases with a fitted transition temperature T_{C2} of ~ 343 K (denoted by Δ_2). Notably, the CDW gap Δ_2 shows a highly anisotropic momentum dependence, which has no trace near the Γ point (at the α point) but can be clearly observed near the M point (at the β point).

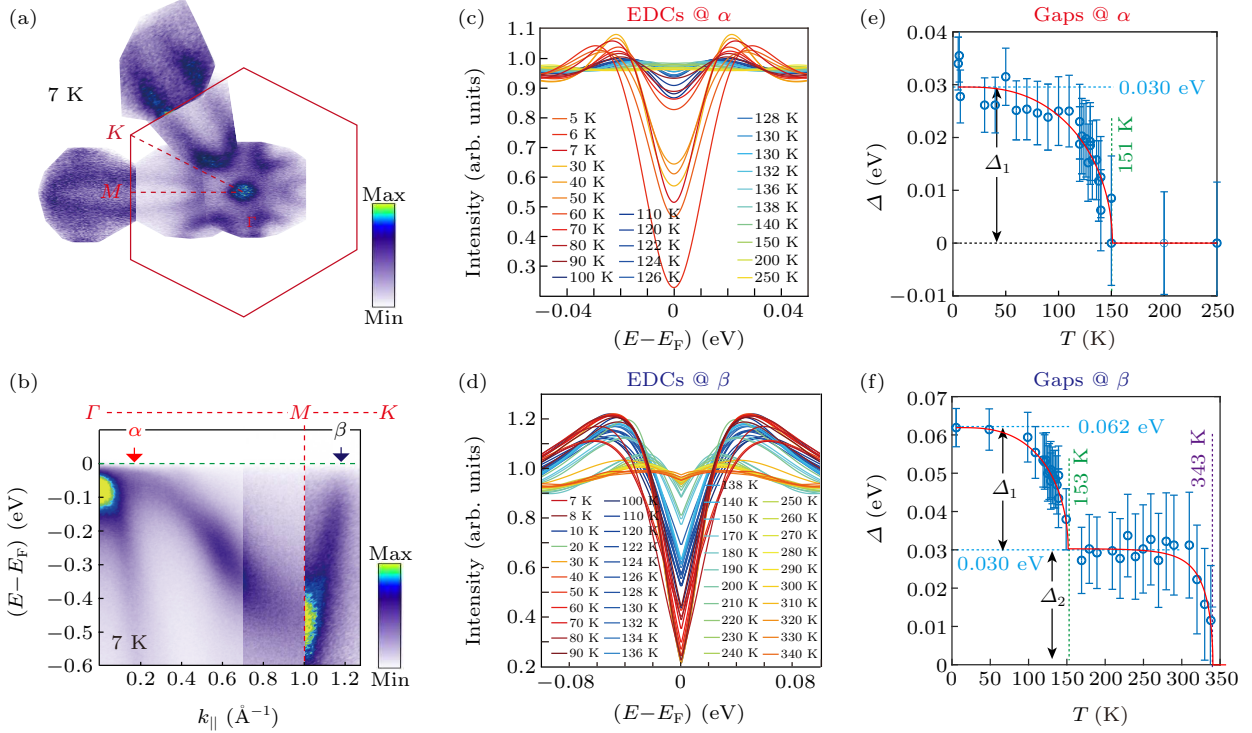


Fig. 4. (a) BZ and constant-energy-mapping of the monolayer 1T-VSe₂ at the binding energy of -0.1 eV taken at 7 K. (b) ARPES spectra along the Γ - M - K directions taken at 7 K. (c) and (d) Symmetrized EDCs at different temperatures at the momentum positions marked as the α and β points in panel (b), respectively. The different colored lines represent the different temperatures. (e) Temperature dependence of the CDW gap extracted from the symmetrized EDCs at the momentum position marked as the α point. The red line is the fitting result from Eq. (1) using a single Δ_1 . The blue and green dashed lines indicate the fitting results of $\Delta_1 = 30 \pm 6$ meV and $T_{C1} = 151 \pm 6$ K, respectively. (f) Temperature dependence of the CDW gap extracted from the symmetrized EDCs at the momentum position marked as the β point. The red line is the fitting result from Eq. (1) using a total $\Delta(T) = \Delta_1(T) + \Delta_2(T)$. The blue dashed lines indicate the fitting results of $\Delta_1 = 32 \pm 2$ meV and $\Delta_2 = 30 \pm 1$ meV, and the green and purple dashed lines indicate the fitting results of $T_{C1} = 153 \pm 2$ K and $T_{C2} = 343 \pm 2$ K, respectively. The errors of the fitting results are in 68% confidence interval. The error bars of the gaps data are set as $\sqrt{(\frac{1}{2}k_B T)^2 + (\epsilon_s)^2}$, where k_B is the Boltzmann constant, ϵ_s is the resolution limit (~ 5 meV) of the ARPES system.

With the two-gap form, we can go further to make a comparison to the experimental ARPES spectra by using the phenomenological self-energy expression developed originally for high- T_C cuprates,^[51]

$$\Sigma(\mathbf{k}, \omega) = -i\Gamma_1 + \frac{\Delta(T)^2}{[\omega + \epsilon(\mathbf{k}) + i\Gamma_0]}, \quad (2)$$

where $\Delta(T)$ is the CDW gap, Γ_1 the single-particle scattering rate, Γ_0 the inverse particle-hole pair lifetime, and $\epsilon(\mathbf{k})$ the single-particle dispersion. Using Eq. (2), we can calculate the single-particle spectral function $A(\mathbf{k}, \omega)$ via the Green's function as $A(\mathbf{k}, \omega) = -\text{Im}G(\mathbf{k}, \omega)/\pi$ with $G(\mathbf{k}, \omega) = [\omega - \epsilon(\mathbf{k}) - \Sigma(\mathbf{k}, \omega)]^{-1}$. In our numerical calculations, $\epsilon(\mathbf{k})$ is obtained by the tight-binding fit to the first-principles calculations for 1T-VSe₂ (see Section 2), and $\Gamma_1 = 0.005$ eV and $\Gamma_0 = 0.005$ eV are chosen. Figures 5(a)–

5(f) show the calculated spectral functions along the M - Γ - M and K - M - K directions at 343 K, 200 K, and 7 K, respectively. Figures 5(g)–5(l) are the experimental ARPES data at 340 K, 200 K, and 7 K, respectively. The calculated spectra show a good agreement to the experimental results. At 343 K, both the Δ_1 and Δ_2 equal zero according to Eq. (1), and the calculated spectra functions show no gap along both Γ - M and M - K directions [see Figs. 5(a) and 5(b)], and ARPES spectra at 340 K show no gap along the Γ - M direction [see Fig. 5(g)], and a tiny gap that is smaller than the resolution limit and difficult to be directly distinguished along the M - K direction [see Fig. 5(h)]. When the temperature is reduced to be 200 K, Δ_1 keeps zero but Δ_2 becomes nonzero. Since Δ_2 only exists along the M - K direction, the band along the M - K direction opens a small gap

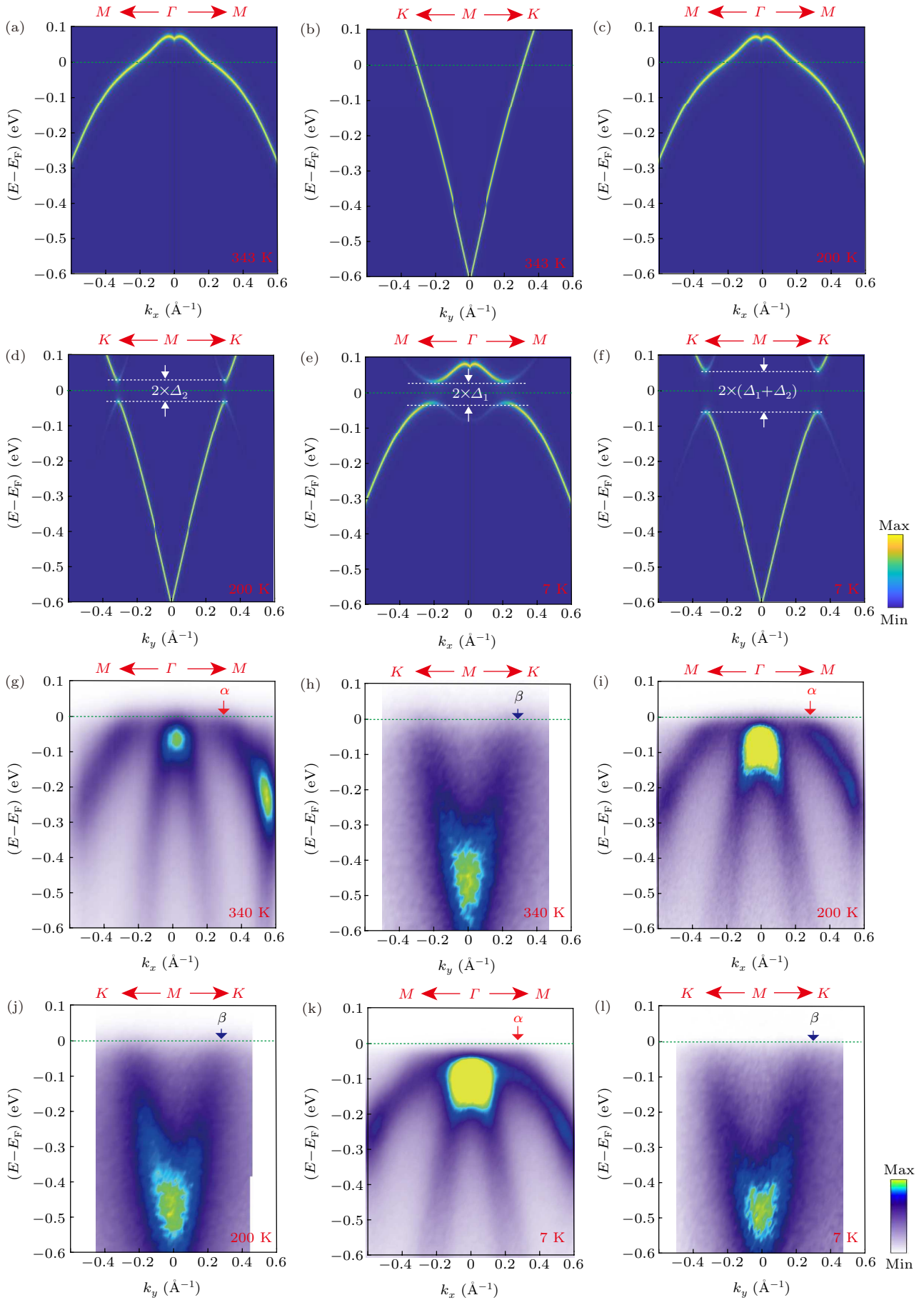


Fig. 5. (a)–(f) Calculated spectral function at selected temperatures along the M – Γ – M and K – M – K directions. (g)–(l) ARPES spectra along the M – Γ – M and K – M – K directions scanned at the corresponding temperatures experimentally.

at the Fermi level [Figs. 5(d) and 5(j)] but the band along the Γ – M direction still shows no gap [Figs. 5(c) and 5(i)]. When the temperature is further reduced [to be 7 K], both Δ_1 and Δ_2 becomes nonzero. Since Δ_1 exists in both the Γ – M and M – K directions while Δ_2 not, thus the band along the M – K direction shows a larger gap [Figs. 5(f) and 5(l)] than that along the Γ – M direction at the Fermi level [Figs. 5(e) and 5(k)].

We note that some previous works on the CDW gap in monolayer 1T-VSe₂ also reported a similar two-step gap transition,^[27,32] but they attributed one step of the gap transition to the metal–insulator transition^[27] or the pseudogap.^[32] Differently, with the unveiling of the hidden incommensurate CDW order, here we suggest the CDW gap consisted of two gap parts ($\Delta_1 + \Delta_2$), which gives a well explanation and a comprehensive description on the two-step CDW transition. Interestingly, a similar two-stage CDW transition associated with the incommensurate CDW phase was also reported in the cuprates of La_{2–x}Ba_xCuO₄.^[47] Besides, we note that by simply treating the scattering rates Γ_1 and Γ_0 as constants in our calculations when using Eq. (2), we get a good agreement to the experimental data. It suggests that the single-particle scattering rate Γ_1 and the inverse pair lifetime Γ_0 may show less or even no temperature dependence, and also affect less the CDW phase transitions and gap evolutions in monolayer 1T-VSe₂. This is in contrast to the case in high- T_C cuprates,^[51] where both Γ_1 and Γ_0 assumes a strong temperature dependence.

3.3. Discussion on the possible physical mechanism of the CDW phases in monolayer 1T-VSe₂

Previous works have suggested that the ($\sqrt{7} \times \sqrt{3}$) CDW reconstruction can be attributed to the Fermi surface nesting of the elliptic Fermi pockets around the M points in the monolayer 1T-VSe₂,^[31,50] while the proposals for the physical mechanism of the incommensurate CDW phase vary from the imperfect nesting in SmTe₃^[44] to the Coulomb interactions between domain walls, and the inter-layer interaction in monolayer MX₂.^[41] Recent theoretical calculations reveal that the electron–electron correlations, momentum-dependent electron–phonon coupling, together with the Fermi-surface nesting would play important roles in the complicated multiple CDW phases in monolayer VSe₂.^[50,52] In order to investigate the possible physical mechanism of the multiple CDW phases in monolayer VSe₂ from experimental aspect, next we will investigate how the Fermi pockets and the electronic structures evolve during the CDW transition in the following.

Figures 6(a)–6(c) show the secondary differential ARPES spectra taken at 7 K, 200 K, 340 K, respectively. A sharp valence band denoted as the γ band at the Γ point (depicted by the cyan dashed curve) can be clearly observed, showing a movement towards the Fermi level with increasing temperatures. Figure 5(d) show the temperature dependence of the top of the γ band in energy (E_{V1}). We can see that E_{V1} has a linear temperature dependence above ~ 70 K, which can be attributed to the temperature-dependent charge transfer from the substrate to the grown film. The movement of the γ band in energy will affect the shape and size of the elliptic

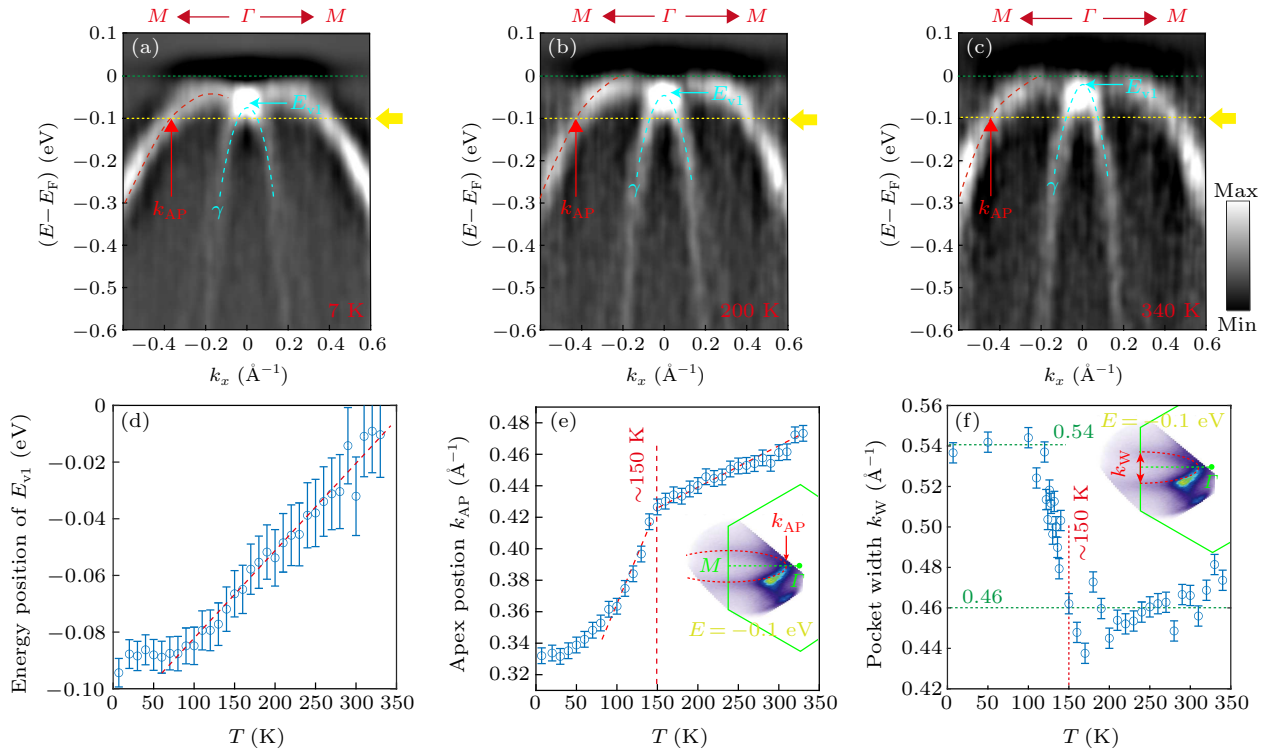


Fig. 6. (a)–(c) Secondary differential spectra along the M – Γ – M directions taken at 7 K, 200 K, and 340 K respectively. (d) The temperature dependence of the γ band maximum E_{V1} . (e) The temperature dependence of the momentum position of the pocket apex (k_{AP}). The inset is the constant-energy-mapping at -0.1 eV and the position of k_{AP} . (f) The temperature dependence of the width of the elliptic pocket around the M point (k_W), the inset indicates the k_W in the constant-energy-mapping at -0.1 eV.

Fermi pockets around the M point profoundly. To evaluate the changing of the elliptic Fermi pockets, we plot the temperature dependence of the momentum positions of the pocket apex (k_{AP}) and the pocket widths (k_W) in Figs. 6(e) and 6(f), respectively. Notably, k_{AP} also moves monotonically with the increasing of temperature, but exhibits a distinct kink around ~ 150 K (see the red dashed lines). While k_W shows nearly no temperature dependence until a little bit less than 150 K, then exhibits a step-like drop around ~ 150 K. Since the $(\sqrt{7} \times \sqrt{3})$ CDW phase was considered due to the Fermi nesting of these elliptic Fermi pockets,^[31,50] and the Fermi nesting vectors are highly depending on the size and shape of the elliptic Fermi pockets, thus we suggest that the changing of the pocket shape (k_{AP}) and the shrinking of the pocket size (k_W) with increasing temperature will destroy the nesting wave vector of $(\sqrt{7} \times \sqrt{3})$, resulting the disappearance of the $(\sqrt{7} \times \sqrt{3})$ phase at the high temperatures of 165 K and 300 K in the STM images and the closing of the CDW gap Δ_1 above ~ 150 K. However, the formation of the incommensurate CDW phase was believed not to be related to the Fermi surface nesting.^[41,44] Therefore, the changing of the elliptic Fermi pockets will not eliminate the incommensurate CDW phase and the gap Δ_2 above ~ 150 K, but only slightly affect the formations of the stripe-like incommensurate CDW order and the corresponding wave vectors. When the temperature is above $T_{C2} = 343$ K, the thermo fluctuation has an energy scale of $k_B T_{C2} \approx 30$ meV, which is same to the value of $\Delta_2 = 30 \pm 1$ meV. Even though we did not directly observe the closing of the CDW gap at the β point at 340 K, but the gap closing trend around the 340 K suggested that the incommensurate CDW gap would be suppressed by the thermo fluctuation that has a same energy scale to the Δ_2 .

4. Conclusion

In summary, we unveil a hidden stripe-like incommensurate ($\sim 2a$) CDW phase behind the $(\sqrt{7} \times \sqrt{3})$ CDW phase in the epitaxial monolayer 1T-VSe₂ film. The co-existence and interference between the hidden incommensurate CDW phase and the $(\sqrt{7} \times \sqrt{3})$ phase result the short-range $(\sqrt{7} \times \sqrt{3})$ and $(2 \times \sqrt{3})$ CDW reconstructions at 4 K. Using the VT/RT-STM measurements, we found that the $(\sqrt{7} \times \sqrt{3})$ CDW will disappear at 165 K, but the incommensurate CDW phase can survive even at room temperature. Combining the ARPES measurements and theoretical analysis, we suggest that these two CDW phases exhibit a two-step CDW gap transition. Such similar two-step gap transition has also been reported but with different explanations of metal-insulator transition^[27] or pseudogap.^[32] Significantly, here we suggested that the CDW gap consists of two parts, one is corresponding to the $(\sqrt{7} \times \sqrt{3})$ reconstruction results a full gap part $\Delta_1 \sim 32$ meV with a transition temperature $T_{C1} \sim 153$ K, while the other

is corresponding to the incommensurate CDW order shows a highly momentum dependence and results a partial gap structure $\Delta_2 \sim 30$ meV with a transition temperature $T_{C1} \sim 343$ K. Our results illustrate an unusual CDW phenomenon with multiple reconstruction phases and a two-step CDW gap transition in the epitaxial monolayer 1T-VSe₂, giving a deep and comprehensive understanding on the CDW mechanism in monolayer 1T-VSe₂.

Acknowledgments

Project supported by the National Natural Science Foundation of China (Grant Nos. 92165205, 11790311, 12004172, 11774152, 11604366, and 11634007), the National Key Research and Development Program of China (Grant Nos. 2018YFA0306800 and 2016YFA0300401), the Program of High-Level Entrepreneurial and Innovative Talents Introduction of Jiangsu Province, the Jiangsu Planned Projects for Postdoctoral Research Funds (Grant No. 2020Z172), and the Natural Science Foundation of Jiangsu Province, China (Grant No. BK 20160397).

Appendix A: Symmetrized EDCs around transition temperatures

The symmetrized EDCs around the transition temperatures are shown in the following figures.

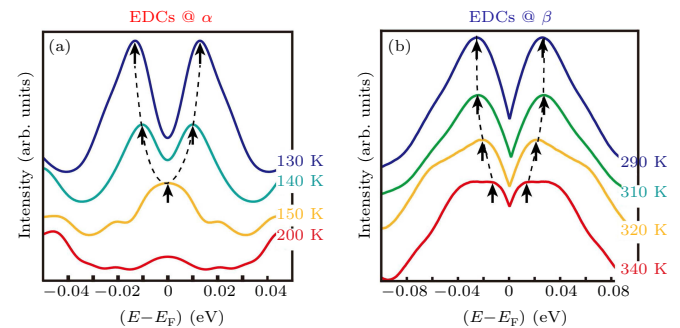


Fig. A1. Symmetrized EDCs around the transition temperature T_{C1} (a) and T_{C2} (b). The black arrows and dashed lines indicate the close and closing trend of the gap around the transition temperatures.

References

- [1] Manzeli S, Ovchinnikov D, Pasquier D, Yazyev O V and Kis A 2017 *Nat. Rev. Mater.* **2** 17033
- [2] Khan K, Tareen A K, Aslam M, Wang R H, Zhang Y P, Mahmood A, Ouyang Z B, Zhang H and Guo Z Y 2020 *J. Mater. Chem. C* **8** 387
- [3] Xu M, Liang T, Shi M and Chen H 2013 *Chem. Rev.* **113** 3766
- [4] Novoselov K S, Mishchenko A, Carvalho A and Castro Neto A H 2016 *Science* **353** aac9439
- [5] Butler S Z, Hollen S M, Cao L, *et al.* 2013 *ACS Nano* **7** 2898
- [6] Kumar A and Ahluwalia P K 2012 *Euro. Phys. J. B* **85** 186
- [7] Qian X, Liu J, Fu L and Li J 2014 *Science* **346** 1344
- [8] Ugeda M M, Bradley A J, Shi S F, Da Jornada F H, Zhang Y, Qiu D Y, Ruan W, Mo S K, Hussain Z, Shen Z X, Wang F, Louie S G and Crommie M F 2014 *Nat. Mater.* **13** 1091
- [9] Ugeda M M, Bradley A J, Zhang Y, Onishi S, Chen Y, Ruan W, Ojedara-Aristizabal C, Ryu H, Edmonds M T, Tsai H Z, Riss A, Mo S K, Lee D, Zettl A, Hussain Z, Shen Z X and Crommie M F 2016 *Nat. Phys.* **12** 92

- [10] Xi X X, Zhao L, Wang Z F, Berger H, Forro L, Shan J and Mak K F 2015 *Nat. Nanotechnol.* **10** 765
- [11] Xi X X, Wang Z F, Zhao W W, Park J H, Law K T, Berger H, Forro L, Shan J and Mak K F 2016 *Nat. Phys.* **12** 139
- [12] Wang Q Y, Li Z, Zhang W H, Zhang Z C, Zhang J S, Li W, Ding H, Ou Y B, Deng P, Chang K, Wen J, Song C L, He K, Jia J F, Ji S H, Wang Y Y, Wang L L, Chen X, Ma X C and Xue Q K 2012 *Chin. Phys. Lett.* **29** 037402
- [13] He S L, He J F, Zhang W H, *et al.* 2013 *Nat. Mater.* **12** 605
- [14] Tang S, Zhang C, Wong D, *et al.* 2017 *Nat. Phys.* **13** 683
- [15] Chen P, Pai W W, Chan Y H, Sun W L, Xu C Z, Lin D S, Chou M Y, Fedorov A V and Chiang T C 2018 *Nat. Commun.* **9** 2003
- [16] Wu S, Fatemi V, Gibson Q D, Watanabe K, Taniguchi T, Cava R J and Jarillo-Herrero P 2018 *Science* **359** 76
- [17] Chen P, Chan Y H, Fang X Y, Zhang Y, Chou M Y, Mo S K, Hussain Z, Fedorov A V and Chiang T C 2015 *Nat. Commun.* **6** 8943
- [18] Ryu H, Chen Y, Kim H, Tsai H Z, Tang S J, Jiang J, Liou F, Kahn S, Jia C H, Omrani A A, Shim J H, Hussain Z, Shen Z X, Kim K, Min B I, Hwang C, Crommie M F and Mo S K 2019 *Nano Lett.* **19** 626
- [19] Campi D, Bernasconi M and Benedek G 2012 *Phys. Rev. B* **86** 075446
- [20] Yu S J, Zhang J T, Tang Y and Ouyang M 2015 *Nano Lett.* **15** 6282
- [21] Lee H 2016 *J. Electron. Mater.* **45** 1115
- [22] Rossnagel K 2011 *J. Phys.: Condens. Matter* **23** 213001
- [23] Chen C W, Choe J and Morosan E 2016 *Rep. Prog. Phys.* **79** 084505
- [24] Eaglesham D J, Withers R L and Bird D M 1986 *J. Phys. C-Solid State Phys.* **19** 359
- [25] Jolie W, Knispel T, Ehlen N, Nikonov K, Busse C, Gruneis A and Michely T 2019 *Phys. Rev. B* **99** 115417
- [26] Strocov V N, Shi M, Kobayashi M, Monney C, Wang X, Krempasky J, Schmitt T, Patthey L, Berger H and Blaha P 2012 *Phys. Rev. Lett.* **109** 086401
- [27] Duvjir G, Choi B K, Jang I, Ulstrup S, Kang S, Ly T T, Kim S, Choi Y H, Jozwiak C, Bostwick A, Rotenberg E, Park J G, Sankar R, Kim K S, Kim J and Chang Y J 2018 *Nano Lett.* **18** 5432
- [28] Chua R, Yang J, He X, Yu X, Yu W, Bussolotti F, Wong P K J, Loh K P, Breese M B H, Goh K E J, Huang Y L and Wee A T S 2020 *Adv. Mater.* **32** 2000693
- [29] Chua R, Henke J, Saha S, Huang Y L, Gou J, He X, Das T, Wezel J V, Soumyanarayanan A and Wee A T S 2022 *ACS Nano* **16** 783
- [30] Feng J G, Biswas D, Rajan A, *et al.* 2018 *Nano Lett.* **18** 4493
- [31] Chen P, Pai W W, Chan Y H, Madhavan V, Chou M Y, Mo S K, Fedorov A V and Chiang T C 2018 *Phys. Rev. Lett.* **121** 196402
- [32] Umemoto Y, Sugawara K, Nakata Y, Takahashi T and Sato T 2019 *Nano Res.* **12** 165
- [33] Wang Q, Zhang W, Wang L, He K, Ma X and Xue Q 2013 *J. Phys.: Condens. Matter* **25** 095002
- [34] Giannozzi P, Baroni S, Bonini N, *et al.* 2009 *J. Phys.: Condens. Matter* **21** 395502
- [35] Perdew J P, Burke K and Ernzerhof M 1996 *Phys. Rev. Lett.* **77** 3865
- [36] Esters M, Hennig R G and Johnson D C 2017 *Phys. Rev. B* **96** 235147
- [37] Chen W, Xie X, Zong J, Chen T, Lin D, Yu F, Jin S, Zhou L, Zou J, Sun J, Xi X and Zhang Y 2019 *Sci. Rep.* **9** 2685
- [38] Xie X, Ding Y, Zong J, Chen W, Zou J, Zhang H, Wang C and Zhang Y 2020 *Appl. Phys. Lett.* **116** 193101
- [39] Hovden R, Tsen A W, Liu P, Savitzky B H, El Baggari I, Liu Y, Lu W, Sun Y, Kim P, Pasupathy A N and Kourkoutis L F 2016 *Proc. Nat. Acad. Sci.* **113** 11420
- [40] Lim S, Kim J, Won C and Cheong S W 2020 *Nano Lett.* **20** 4801
- [41] Nakatsugawa K, Tanda S and Ikeda T N 2020 *Sci. Rep.* **10** 1239
- [42] Yang H X, Cai Y, Ma C, Li J, Long Y J, Chen G F, Tian H F, Wei L L and Li J Q 2016 *Europhys. Lett.* **114** 67002
- [43] Fang A, Ru N, Fisher I R and Kapitulnik A 2007 *Phys. Rev. Lett.* **99** 046401
- [44] Gweon G H, Denlinger J D, Clack J A, Allen J W, Olson C G, Dimasi E, Aronson M C, Foran B and Lee S 1998 *Phys. Rev. Lett.* **81** 886
- [45] Shi Z, Kuhn S J, Flicker F, Helm T, Lee J, Steinhardt W, Dissanayake S, Graf D, Ruff J, Fabbri G, Haskel D and Haravifard S 2020 *Phys. Rev. Res.* **2** 042042
- [46] Lee J, Nagao M, Mizuguchi Y and Ruff J 2021 *Phys. Rev. B* **103** 245120
- [47] Miao H, Fumagalli R, Rossi M, Lorenzana J, Seibold G, Yakhov-Harris F, Kummer K, Brookes N B, Gu G D, Braicovich L, Ghiringhelli G and Dean M P M 2019 *Phys. Rev. X* **9** 031042
- [48] Chen W, Hu M, Zong J, Xie X, Meng Q, Yu F, Wang L, Ren W, Chen A, Liu G, Xi X, Li F-S, Sun J, Liu J and Zhang Y 2021 *Adv. Mater.* **33** 2004930
- [49] Cudazzo P, Gatti M and Rubio A 2014 *Phys. Rev. B* **90** 205128
- [50] Jang I, Duvjir G, Choi B K, Kim J, Chang Y J and Kim K S 2019 *Phys. Rev. B* **99** 014106
- [51] Norman M R, Randeira M, Ding H and Campuzano J C 1998 *Phys. Rev. B* **57** R11093
- [52] Si J G, Lu W J, Wu H Y, Lv H Y, Liang X, Li Q J and Sun Y P 2020 *Phys. Rev. B* **101** 235405